Macromolecules

ARTICLE

pubs.acs.org/Macromolecules

Dispersion Morphology of Poly(methyl acrylate)/Silica Nanocomposites

Dustin W. Janes,[†] Joseph F. Moll,[‡] Shane E. Harton,[†] and Christopher J. Durning*[,†]

[†]Department of Chemical Engineering, Columbia University MC 4721, 500 W. 120th Street, Room 801 S. W. Mudd Hall, New York, New York 10027, United States

[‡]Department of Chemistry, Columbia University, MC 3178, 3000 Broadway New York, New York 10027, United States

Supporting Information

ABSTRACT: Nearly monodisperse poly(methyl acrylate) (PMA) and spherical SiO_2 nanoparticles (NP, $d = 14 \pm 4$ nm) were co-cast from 2-butanone, a mutually good solvent and a displacer of adsorbed PMA from silica. The effects of NP content and post-casting sample history on the dispersion morphology were found by small-angle X-ray scattering supplemented by transmission electron microscopy. Analysis of the X-ray results show that cast and thermally annealed samples exhibited a nearly random particle dispersion. That the same samples, prior to annealing, were not well-dispersed is indicative of thermodynamic miscibility during thermal annealing over the range of NP loadings studied. A simple mean-field thermodynamic model suggests that miscibility results primarily from favorable polymer segment/NP surface interactions. The model also indicates, and experiments confirm, that subsequent exposure of the composites to the likely displacer ethyl acetate results in entropic destabilization and demixing into NP-rich and NP-lean phases.

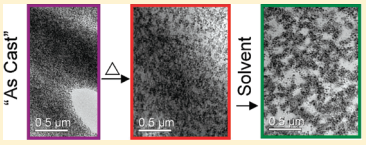

I. INTRODUCTION

Nanoparticles embedded in a polymeric matrix produce polymer "nanocomposites" (PNCs) which can exhibit unique properties.[1,2] The early literature on nylon PNCs provides a good example. Dramatic alteration of the mechanical properties, thermal stability, and gas barrier characteristics result from the addition of relatively small amounts (2−6 wt %) of montmorillonite clay.[3,4] At least some of the property enhancements unique to PNCs are due to alteration of the matrix material near the nanoparticle surface, which can contribute importantly since the internal surface area in PNCs is very large relative to composites made with micrometer-sized filler (a factor of 10^2−10^3 larger). Consider, for example, a PNC with monodisperse spherical nanoparticles of diameter d and volume fraction ϕ_P. If there exists an altered interfacial layer of thickness δ surrounding each nanoparticle, then the volume fraction of interfacial material in the matrix, ϕ_δ, is given by

$$\phi_\delta = \left[\left(1+\frac{2\delta}{d}\right)^3 - 1\right]\phi_P \qquad (1)$$

for dilute ($\phi_P + \phi_\delta \ll 1$), noninteracting particles. Although not quantitatively valid for real systems with $\phi_P + \phi_\delta \geq 10^{-1}$, eq 1 anticipates that ϕ_δ becomes significant even at very low ϕ_P when d and δ are comparable. For example, according to eq 1 for a PNC with $d \cong \delta \cong 10$ nm the matrix is dominated by interfacial material when ϕ_P approaches only $\cong$ 4%! This makes clear that relatively small loadings of nanoparticles have the *potential* to alter certain properties of the matrix material significantly through the influence of a very large internal surface area.

While addition of nanoparticles to a polymer can lead to unexpected property changes, the details can also depend strongly on the spatial distribution of nanoparticles in the composite. For example, Takahashi and Paul[5,6] showed that the gas selectivity of poly(ether imide) deteriorated when added silica nanoparticles formed large, low-aspect-ratio aggregates but could be maintained when the added nanoparticles were better dispersed. In another example, Akcora et al.[7] reported much better mechanical reinforcement of polystyrene (PS) with spherical silica nanoparticles bearing grafted PS at low nanoparticle content, when the filler formed sheetlike aggregates compared to when the filler was uniformly dispersed or formed dense, roughly spherical aggregates. Advances in many emerging PNC applications, such as membranes[5,6] and PNC photovoltaics for solar cells,[8] demand an understanding and control of the factors influencing dispersion morphology. Unfortunately, PNC morphology control remains an unresolved challenge. For example, Schaefer and Justice[9] report similar fractal long-range disorder in the dispersion morphology of PNCs despite a broad range of materials selection and PNC preparation schemes.

This work focuses on a model polymer melt/nanoparticle composite system. We aim to clarify the role of thermochemical history on the resulting composite morphology, thereby contributing toward PNC morphology control in melt/nanoparticle composite systems. Polymer melts and nanoparticles are susceptible to demixing, leading to a nanoparticle dense "phase" or

Received: January 29, 2011
Revised: April 22, 2011
Published: May 18, 2011

nanoparticle aggregates. This is due to a weak entropy of mixing (relative to small molecule mixtures) and particle−particle attractions from the van der Waals forces. These effects can be aggravated by unfavorable polymer segment−nanoparticle surface interactions and (possibly) attractive depletion forces. Several strategies to achieve good dispersion of nanoparticles in polymer melts are indicated in the literature. Chemical modification of the particle surface to improve polymer segment−nanoparticle surface interactions can make the enthalpy of mixing favorable and aid in dispersion.[10,11] Also, coating of the particle surface with polymers, by either grafting[12] or physisorption,[13] can mediate or prevent nanoparticle agglomeration by the resulting short-range interparticle repulsive forces. Several groups[14−18] have developed simple mean-field expressions for the free energy of mixing of a polymer melt/nanoparticle pair which capture these and other effects and allow construction of phase diagrams for such PNCs, indicating conditions favoring demixing and therefore the formation of nanoparticle-rich phases. For example, Hooper and Schweizer[11] examined the miscibility in polymer melt/nanoparticle mixtures using the polymer reference interaction site model (PRISM). They find that the relatively weak entropy of mixing together with sufficiently attractive polymer segment−nanoparticle surface interactions can lead to miscibility, especially for polymers that are not so long to enable effective interparticle attractions through significant bridging. These studies suggest that miscibility in PNCs from polymer melts can be controlled over wide ranges of ϕ_P by careful choice of a polymer−nanoparticle pair, with miscibility being favored by attractive segment−surface site interactions, relatively small particle size, and relatively short polymer length. Relatively few studies of melt/nanoparticle dispersion morphologies (for example, refs 12, 14, 17, and 19−21) provide direct comparisons between experimental and theoretical results. This paper provides a comparison between experimentally measured PNC dispersion morphologies and theoretical phase diagrams to help understand the competitive roles of mixing entropy, interparticle attractions, and polymer segment−particle surface contact energies.

We report on PNCs of nearly monodisperse poly(methyl acrylate) (PMA) and spherical silica nanoparticles. Samples are fabricated by co-casting from solution in 2-butanone (MEK). MEK is a mutually good solvent for the polymer and particles and also a displacer of PMA from silica,[22] enabling simple, reproducible sample preparation by solvent casting without gelation at high particle density via bridging of particles by adsorbed polymer. This polymer−particle pair likely exhibits physisorption of polymer from the melt through hydrogen bonding between carbonyl groups of the PMA repeat unit and silanol groups on the silica surface.[23,24] We therefore anticipate favorable polymer segment−particle surface site interactions which could promote good dispersion of nanoparticles into the melt. After casting from MEK, the PNC samples are subject to several well-defined thermochemical histories to discern their effects on the dispersion morphology. To determine the latter, we rely primarily on small-angle X-ray scattering (SAXS) with additional support from transmission electron microscopy (TEM).

II. EXPERIMENTAL SECTION

Materials. All materials were used as-received. Certified ACS grade ethyl acetate was purchased from Fisher Chemical (Fairlawn, NJ), and 2-butanone (MEK, 99+%), was purchased from Acros Organics (Geel, Belgium). The antioxidant Irganox 1010 was supplied by Ciba (Basel, Switzerland). Silica (SiO_2) nanoparticles suspended in 2-butanone (Organosilicasol MEK-ST) were supplied by Nissan Chemical America (Houston, TX). The silica nanoparticles were characterized by the manufacturer using electron microscopy as polydisperse spheres with diameters in the range 10−15 nm (MEK-ST). The suspension was specified as 30−31 wt % silica and was stored at 5 °C.

Poly(methyl acrylate) (PMA, M_w = 55 960, M_n/M_w = 1.04) was synthesized via atom transfer radical polymerization (ATRP). The synthesis procedure was similar to that employed by Xia and Matyjaszewski.[25] 132 mg of CuBr catalyst was placed in a 300 mL flask. 100 mL of methyl acrylate was passed through a basic alumina column and into the flask. 190 μL of PMDETA (pentamethyldiethylenetriamine) was added to the solution, which was then sealed with a rubber septum. To remove oxygen, the flask was then purged with nitrogen gas for 5 min followed by bubbling nitrogen gas through the solution for 25 min. 120 μL of initiator (methyl α-bromoisobutyrate) was injected into the flask. The homogeneous solution was immersed in an oil bath held at 70 °C with constant stirring at 400 rpm via a magnetic stir bar for 7.25 h. After cooling in an ice water bath, about 150 mL of tetrahydrofuran was added. The solution was then passed through a neutral alumina column to remove the catalyst and precipitated into hexanes, filtered, and dried under vacuum. Molecular weight characterization was done by gel permeation chromatography using PMMA standards for calibration.

Preparation of PNCs. PNC films were co-cast from semi-dilute solutions of PMA in MEK with added silica nanoparticles, according to a procedure similar to one used previously to yield well-dispersed PNCs made from poly(2-vinylpyridine) and silica.[26] After evaporation of the solvent the films were annealed by one of several procedures to provide a well-defined sample history. To achieve good mixing during preparation, we employed a 750 W probe ultrasonicator fitted with a tapered tip (Ultrasonic Processor, model GEX-750 fitted with a model CV33 probe) and operated it at 24% of the maximum amplitude with 2 s pulses followed by a 1 s rest. Details of the composite preparation are as follows.

First, solutions of PMA (50−250 mg/mL) and Irganox 1010 (20 mg/mL) in MEK were prepared in Teflon-capped vials. The Irganox 1010 was added 0.1 wt % relative to polymer to minimize oxidation during subsequent thermal annealing. The as-received silica dispersion MEK-ST was diluted with MEK 2:1, resulting in silica MEK solutions of about 200 mg/mL. This was shaken for about a minute and then sonicated for 3 min. Appropriate amounts of the silica solution were then added to polymer/antioxidant solutions to produce polymer and silica together in MEK with a known weight ratio. The composite solutions were then shaken for several minutes and sonicated in pulse mode for about 1 min, meaning that the polymer experienced high-energy sonications for a total of only about 40 s. This short sonication time was chosen to avoid polymer degradation; for example, a sonication time of 2 min has been shown to reduce the molecular weight of polystyrene (M_w = 92 000 g/mol) by only 2% without affecting its polydispersity.[27]

The use of MEK provides a critical advantage in the PNC preparation procedure because it is both a good solvent for the two components and a displacer of adsorbed PMA chains from the silica surface.[22] If the casting solvent is not a displacer, physisorption of polymer to silica takes place in solution and can result in an intractable gel unsuitable for film casting.[26] For instance, we attempted to duplicate the PNC preparation procedure using 4-methyl-2-pentanone (MIBK) as the casting solvent; MIBK is not a displacer of adsorbed PMA chains from the silica surface.[22] These PNC solutions immediately became cloudy after mixing, consistent with nanoparticle aggregation in solution presumably caused by adsorbing PMA chains forming "bridges" between particles and could not be cast into uniform thin films. On the other hand, the PNC solutions made in MEK were optically clear and readily formed uniform thin films via drop or spin-casting.

Samples were cast by drying about 200 μL of PNC solution on Teflon sheeting, resulting in films ∼100 μm thick. Three different sets of samples

Table 1. Annealing Procedures

procedure	description
mild thermal annealing	50 °C for 2 days under vacuum ($\approx 10^{-3}$ Torr)
aggressive thermal annealing	150 °C for 2 days under inert gas (N_2) purge
aggressive thermal annealing with subsequent solvent annealing	150 °C for 2 days under inert gas (N_2) purge, followed by exposure to ethyl acetate vapor by keeping the samples in a vented oven with an open container of ethyl acetate at 40 °C for 5 days; the samples were subsequently dried at ambient conditions for 2 days and then thermally annealed at 80 °C for 2 days under vacuum ($\approx 10^{-3}$ Torr)

were prepared for characterization, each undergoing a different annealing procedure as indicated in Table 1. "Mild thermal annealing", "aggressive thermal annealing", and "aggressive thermal annealing with subsequent solvent annealing" were carried out in order to reveal the influence of sample history on the dispersion morphology. The cast and annealed PNC samples do not show any evidence of chemical cross-linking from high-temperature treatment or sonication, as they are easily dissolved by the displacing solvent[22] MEK-but not by toluene for $\phi_P \geq 0.19$, a good solvent for PMA but not a displacer of PMA adsorbed to silica. We consider ethyl acetate, as used in the "aggressive thermal annealing with subsequent solvent annealing" process, to be a likely displacer of adsorbed PMA from silica nanoparticles because it easily dissolves cast and annealed samples.

Characterization Methods. Thermogravimetric analysis (TGA) was performed on a Metter Toledo TGA/SDTA 851 to determine the silica volume fraction, ϕ_P. Small samples (2−20 mg) were added to a clean, tared alumina crucible and were heated from 150 to 1000 °C at a rate of 10 °C/min under nitrogen. From the plot of sample weight vs temperature the sample weight fraction remaining after thermal decomposition, W, was determined. For pure PMA this is denoted W_{PMA}, and for each PNC, W_{PNC}. To correct for the small amount of incombustibles present in the pure PMA, ϕ_P was determined by

$$\phi_P = \frac{\dfrac{W_{PNC} - W_{PMA}}{\rho_{SILICA}}}{\dfrac{W_{PNC} - W_{PMA}}{\rho_{SILICA}} + \dfrac{1 - W_{PNC}}{\rho_{PMA}}} \quad (2)$$

with ρ_{SILICA} and ρ_{PMA} being the mass density of the bulk silica (2.2 g/cm^3) and PMA (1.22 g/cm^3), respectively. On the basis of repeated measurements of W_{PMA} and W_{PNC} and a propagation of uncertainty analysis of eq 2, ϕ_P was determined to within ±0.01 (see Appendix B, Supporting Information). The ϕ_P values determined by TGA were within 4% of those anticipated from the (nominal) weights of polymer and silica added in the PNC preparation procedure.

SAXS was performed on beamline X27C at the National Synchrotron Light Source of Brookhaven National Laboratory (Upton, NY). The monochromatic, pinhole-collimated incident beam had wavelength λ = 0.1371 nm. Silver behenate ($AgC_{22}H_{43}O_2$) was used to calibrate the sample−detector distance. The detector used was a Rayonix MarCCD camera (Evanston, IL). Each experimental run yields an image of the scattered radiation that is reduced by image analysis software (POLAR v.2.6.8, Stonybrook Technology and Applied Research Inc., Stony Brook, NY) to $I(q)$, the intensity of background-subtracted scattered radiation as a function of wave vector q, related to the scattering angle relative to the incident beam, 2θ, by $q = 4\pi\lambda^{-1} \sin\theta$.[28] To model $I(q)$ we applied the "global, unified scattering equation" of Beaucage with a structure factor accounting for correlations of closely packed units,[29] a procedure similar to that of Chen et al.[30] Fitting of this model to the data permitted estimates of a high-order mean nanoparticle radius of gyration, R_{g1}, the spherically normalized polydispersity index,[31] ψ, the average center-to-center interparticle spacing, ζ, and the particle packing factor, k. A brief review of the model, together with a discussion of the physical meaning of the model parameters, and the details of the regression fitting process are given in Appendix A as Supporting Information.

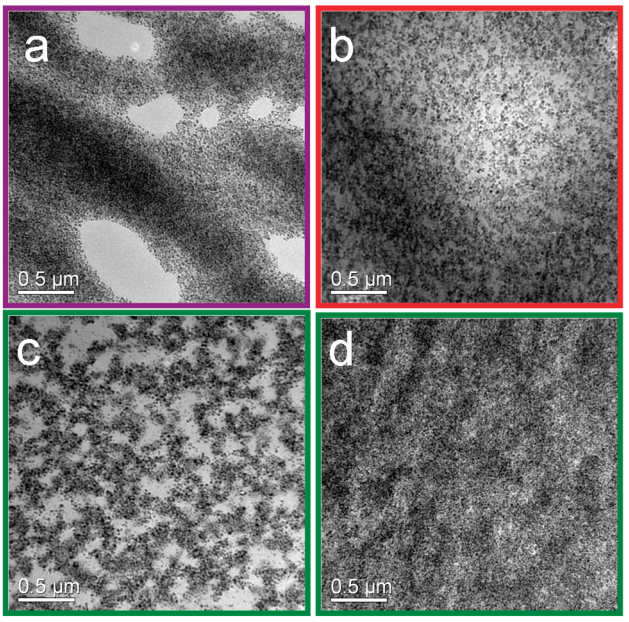

Figure 1. TEM images of samples with silica nanoparticles (d = 10−15 nm). Images a−c have ϕ_P = 0.19 and have undergone the "mild thermal annealing" (a), "aggressive thermal annealing" (b), or "aggressive thermal annealing with subsequent solvent annealing" (c) procedure (Table 1). Image d has ϕ_P = 0.56 and has undergone the "aggressive thermal annealing with subsequent solvent annealing" procedure.

Samples for TEM were prepared by immersing a thin strip of sample within epoxy resin and curing it at 80 °C for 12 h and then ultramicrotoming (UCT, Leica Microsystems, Wetzlar, Germany) 60 ± 10 nm slices, which were floated onto a Formvar-coated copper TEM grid. Representative images at each condition were selected from at least 10 individual images taken with a Philips 430 TEM at 40000× magnification.

III. RESULTS

TEM. Representative TEM images from PNC samples are shown in Figure 1 for ϕ_P = 0.19 and ϕ_P = 0.56. The effect of sample history is illustrated for the ϕ_P = 0.19 samples (Figure 1a−c, see Table 1). Samples that had undergone the "mild thermal annealing" procedure show regions that are highly concentrated in particles in contact with regions where very few particles are present (Figure 1a). The micrographs suggest a demixed state. A more homogeneous distribution of particles is observed for ϕ_P = 0.19 samples that had undergone the "aggressive thermal annealing" procedure (Figure 1b). Demixing is again suggested by the images for samples that had undergone the "aggressive thermal annealing with subsequent solvent annealing" procedure (Figure 1c). However, the size of the particle-rich regions in these samples is

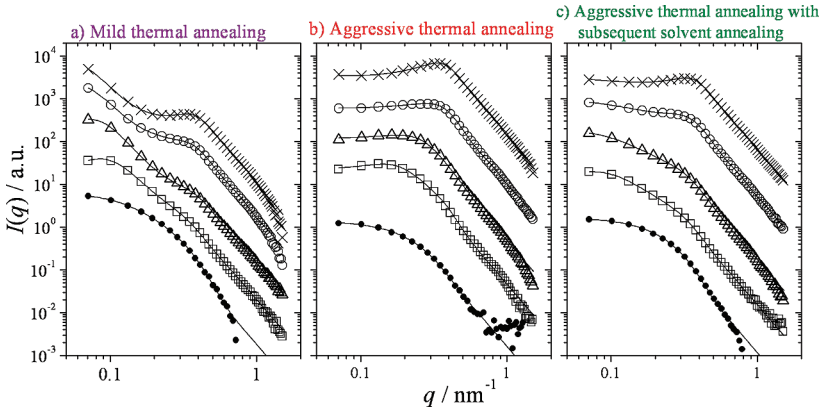

Figure 2. $I(q)$ for composites made with nanoparticles ($d = 10-15$ nm) that had undergone (a) mild thermal annealing, (b) aggressive thermal annealing, or (c) aggressive thermal annealing with subsequent solvent annealing (see Table 1), in which $\phi_P = 0.01$ (●), $\phi_P = 0.06$ (□), $\phi_P = 0.19$ (Δ), $\phi_P = 0.38$ (○), and $\phi_P = 0.51$ (×). For visual clarity, only every eighth data point is displayed. The lines represent the best fit of the model to the data (see Appendix A).

approximately an order of magnitude smaller than for as-cast samples that had undergone the "mild thermal annealing" procedure (Figure 1a). Interestingly, the PNC microstructure in Figure 1c is visually reminiscent of the transient morphologies observed during spinodal decomposition of an immiscible polymer blend quenched to below its upper-critical solution temperature.[32] The sample in which $\phi_P = 0.56$ appears devoid of particle-lean regions (Figure 1d).

Overall, the TEM evidence suggests that PNC samples with the histories "mild thermal annealing" or "aggressive thermal annealing with subsequent solvent annealing" (Figure 1a,c) are demixed into particle-rich and particle-lean regions, although with different morphologies. On the other hand, samples having the "aggressive thermal annealing" history (Figure 1b) evidently exhibit a better dispersion. The small-angle X-ray evidence presented next corroborates this picture.

SAXS. The $I(q)$ data for PNCs with various ϕ_P appear in Figure 2 for samples that have undergone the three different thermochemical histories: "mild thermal annealing", "aggressive thermal annealing", or "aggressive thermal annealing with subsequent solvent annealing" (Table 1). Note that regardless of the annealing procedure, $I(q)$ at $\phi_P = 0.51$ consistently shows a peak at $q \approx 0.35$ nm^{-1}. Modeling indicates this feature results from interparticle correlations arising from strong repulsive interactions at near close packing of nanoparticles at this high ϕ_P. Also, note that $I(q)$ for all samples that had undergone "aggressive thermal annealing" (except for $\phi_P = 0.01$) show a nonzero maximum, suggesting that interparticle correlations are present for these samples even when ϕ_P is relatively low. The model of Beaucage and co-workers[29] fit the data well in all cases over a broad range of q and with physically realistic values of the parameters in all cases (see Appendix A in Supporting Information).

Systematic application of the model allows one to assess the effects of sample history on the dispersion morphology in terms of the model parameters. The results are shown in Figures 3 and 4 which display the fitted model parameters against ϕ_P for the three thermal histories employed. The average center-to-center interparticle spacing, ζ, and the particle radius of gyration, R_{g1} (each in nm), appear in Figure 3. The spherically normalized polydispersity index, ψ,[31] and the particle packing factor, k (both dimensionless), appear in Figure 4. The error bars shown correspond to the 95% confidence limits from the regression fit. In addition, three separate samples were tested at each condition to assess repeatability. Figure 3 shows that the uncertainty and

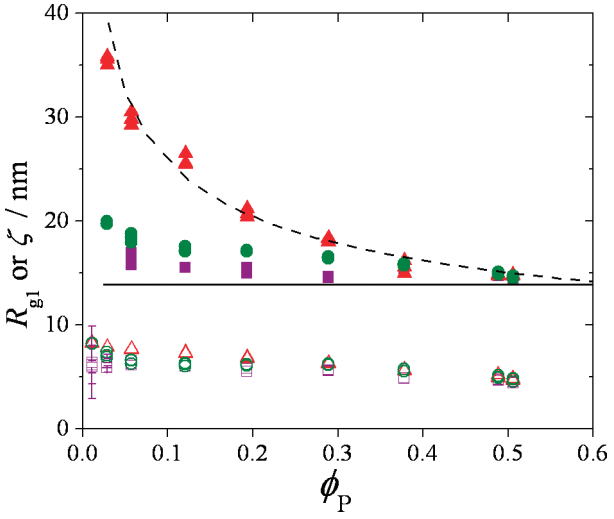

Figure 3. Effects of ϕ_P on the particle radius of gyration R_{g1} (open symbols) and the interparticle spacing ζ (filled symbols) for samples that had undergone mild thermal annealing (■, □), aggressive thermal annealing (▲, △), or aggressive thermal annealing with subsequent solvent annealing (●, ○) (Table 1). The dotted line is $\zeta = \langle d \rangle (0.638/\phi_P)^{1/3}$, valid for randomly dispersed noninteracting spheres with $\langle d \rangle = 13.9$ nm (—). Error bars have been omitted where they are insignificant.

repeatability in ζ and R_{g1} are generally very good. However, for ψ and k they were not consistently good. Because ψ results from the product of six extracted parameters, the uncertainty was large in many cases. In fact, only the samples that had undergone "aggressive thermal annealing" gave reasonably small uncertainties for ψ over the entire range of ϕ_P. The repeatabilities of both ψ and k, however, were significantly worse than those for ζ and R_{g1}.

The most striking result is for the interparticle spacing ζ in samples that have undergone "aggressive thermal annealing" (Figure 3). It decays monotonically from a very high value (≈35 nm) at $\phi_P = 0.03$ to a few nanometers beyond the mean particle diameter at high ϕ_P. On the other hand, ζ remains relatively small, nearly independent of ϕ_P, only decreasing slightly with ϕ_P to just above the mean particle diameter, for samples undergoing the other two thermochemical histories. The results for ζ are consistent with TEM evidence of demixed morphologies for mildly annealed (i.e., as-cast and thermally dried) or solvent-

dx.doi.org/10.1021/ma200205j |Macromolecules 2011, 44, 4920–4927

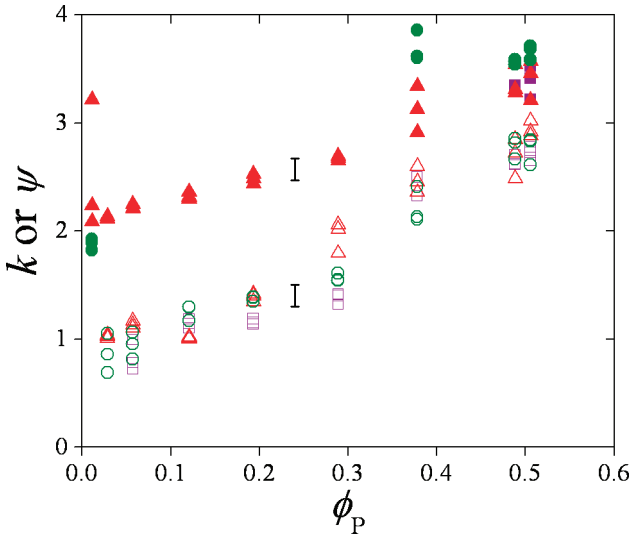

Figure 4. Effects of ϕ_P on the particle packing factor k (open symbols) and the spherically normalized polydispersity index ψ (filled symbols) for samples that had undergone mild thermal annealing (■, □), aggressive thermal annealing (▲, △), or aggressive thermal annealing with subsequent solvent annealing (●, ○) (Table 1). The typical uncertainties (±0.1) for k and ψ are indicated by the error bars.

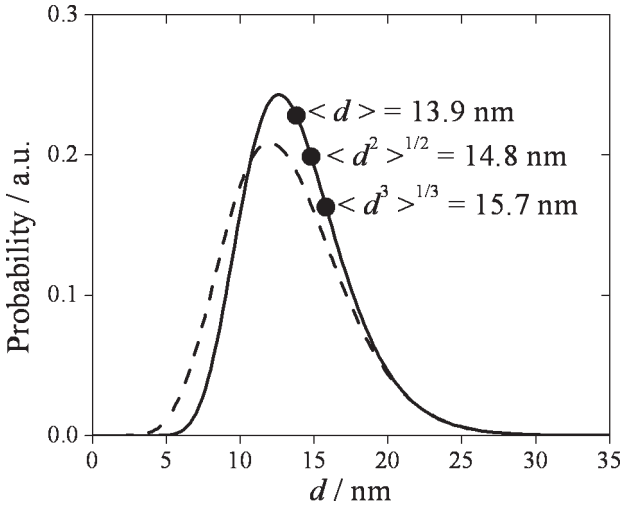

Figure 5. Log-normal (—) and gamma (---) particle size distributions found from the $\phi_P \rightarrow 0$ limits of R_{g1} and ψ for samples that had undergone aggressive thermal annealing (Table 1). Moments found from the log-normal distribution, $\langle d \rangle$ = 13.9 nm, $\langle d^2 \rangle^{1/2}$ = 14.8 nm, and $\langle d^3 \rangle^{1/3}$ = 15.7 nm, are indicated (●).

treated samples, but of near randomly dispersed particles, i.e., of polymer−nanoparticle miscibility, for samples undergoing extensive thermal annealing. In fact, the experimental values of ζ for these samples, which had undergone "aggressive thermal annealing", match those of a simple-minded prediction valid for randomly dispersed spheres without interactions, $\zeta = \langle d \rangle (0.638/\phi_P)^{1/3}$.[33] Thus, the interparticle spacings ζ extracted from SAXS strongly suggests that the silica nanoparticles used here are miscible with PMA after extensive thermal annealing over the whole range of compositions tested. On the other hand, the ζ vs ϕ_P for the samples that had undergone the "aggressive thermal annealing with subsequent solvent annealing" indicates that exposure of initially randomly dispersed composite to ethyl acetate at near unit activity causes aggregation of particles or demixing. Evidently, a kinetically arrested, demixed morphology persists at ambient temperatures after the removal of ethyl acetate during the SAXS experiment.

While R_{g1} and ψ should not change with ϕ_P, the fitted values do vary: R_{g1} decreases weakly with increasing ϕ_P (Figure 3), while values of ψ increase with ϕ_P (Figure 4), but within the range of the parameter's repeatability. We believe contributions to $I(q)$ arising from somewhat larger-size scale structural correlations obscure the scattering by individual nanoparticles, thereby limiting the utility of the model to measure true values of R_{g1} and ψ at high ϕ_P. This artifact has been observed by others.[12,30] For example, Chen et al. report values of R_{g1} extracted from SAXS data with the same model for epoxy/silica nanocomposites that also decrease with ϕ_P.[30] To empirically correct for this, we extrapolated R_{g1} and ψ to $\phi_P = 0$ for near randomly dispersed particles (i.e., for samples subject to "aggressive thermal annealing"), obtaining $R_{g1} = 8.1 \pm 0.1$ nm and $\psi = 2.1 \pm 0.2$. From these values we determined log-normal and gamma particle size distributions consistent with the $I(q)$ data (Figure 5). The resulting log-normal distribution gives the moments $\langle d \rangle$ = 13.9 nm, $\langle d^2 \rangle^{1/2}$ = 14.8 nm, and $\langle d^3 \rangle^{1/3}$ = 15.7 nm. Accordingly, the majority of the particles appear to have d = 10−15 nm as per the manufacturer's specification.

Finally, the fitted values of k increase with ϕ_P as expected ($k = 8\varepsilon\phi_P$), where the constant ε was found to have the (reasonable[34]) value of 0.7.

IV. THEORETICAL INTERPRETATION OF OBSERVED PHASE BEHAVIOR

Here we offer an analysis of two key observations using a mean-field thermodynamic framework: (i) miscibility in the PMA/silica nanoparticle composites after "aggressive thermal annealing" and (ii) apparent demixing of the system in (i) following exposure to the displacer/solvent ethyl acetate at high activity and 40 °C during the "aggressive thermal annealing with subsequent solvent annealing" (see Table 1). To explain these observations, we examine the thermodynamic miscibility criteria using a mean-field expression for the free (Helmholtz) energy of mixing ΔF adapted for our system from two previous models.[17,18] We presume the morphologies observed by SAXS and TEM are those consistent with the phase equilibrium state at the annealing conditions in (i) and (ii) (see Table 1), but kinetically arrested during observation.

To explain finding (i), we consider a melt/nanoparticle mixture, accounting for the possible presence of an adsorbed polymer layer of thickness δ via the parameter $\alpha = (1 + \delta/R)^{-3}$ (see eq 1). Nanoparticles, adsorbed (bound) polymer, and unadsorbed (matrix) polymer have volume fractions ϕ_P, $\phi_P(\alpha^{-1} - 1)$, and $1 - \phi_P\alpha^{-1}$, respectively. Treating the nanoparticles with bound polymer as effectively larger particles, a reasonable formula for ΔF, by a simple extension of the developments in refs 17 and 18, is

$$\frac{v_0 \Delta F}{V k_B T} = \Theta = \frac{1 - \phi_P \alpha^{-1}}{N} \ln(1 - \phi_P) + \chi_{2P} \phi_P (1 - \phi_P) \frac{r_0}{R} + \phi_P \frac{v_0}{v_P} \left[\ln\left(\frac{\phi_P}{\alpha}\right) + \frac{4(\phi_P\alpha^{-1}) - 3(\phi_P\alpha^{-1})^2}{(1 - \phi_P\alpha^{-1})^2} - \ln(\phi_f) - \frac{4\phi_f - 3\phi_f^2}{(1 - \phi_f)^2} \right] + \frac{1}{2} \frac{v_0}{v_P} \left[\frac{\phi_P^2}{v_P} b_{mix} - \frac{\phi_P \phi_f}{v_P} b_f \right] \quad (3)$$

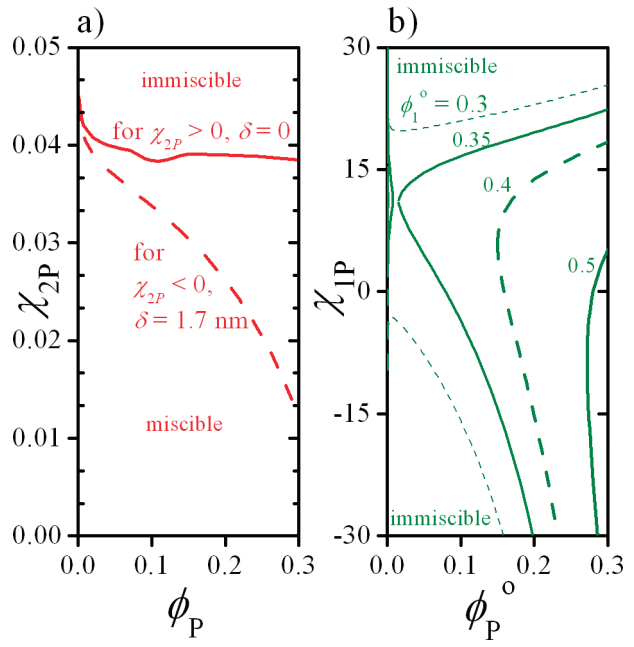

Figure 6. Phase boundaries calculated from eqs 3−7 to represent PNC samples made with smaller nanoparticles (d = 10−15 nm, MEK-ST) during the (a) "aggressive thermal annealing" procedure, in which miscible regions for bound layer thickness $\delta = 0$ (—), $\delta = 1.7$ nm (---) are located below each line, or the (b) "aggressive thermal annealing with subsequent solvent annealing" procedure, in which $\delta = 0$ and miscible regions lie between the lines indicating $\phi_1^\circ = 0.3$ (---), $\phi_1^\circ = 0.35$ (−), $\phi_1^\circ = 0.4$ (− − −), and $\phi_1^\circ = 0.5$ (—).

Here, v_0 and v_P are the volumes for the polymeric repeat unit and nanoparticle, respectively. Estimated values for our system of $v_0 \cong 0.12$ nm^3 and $v_P \cong 2000$ nm^3 are based on radii of r_0 = 0.3 nm and R = 7.9 nm, respectively. The polymer's degree of polymerization is about $N \cong 650$ for the PMA used here.

The first term on the right of eq 3 is the translational entropy of the unbound polymer. The second term is the enthalpic contribution from polymer segment/nanoparticle surface interactions, as formulated by He et al.,[18] using the Flory type parameter χ_{2P}. The third term on the right is the nanoparticle translational entropy, bearing adsorbed polymer, which accounts for the repulsive part of the particle interactions via the Carnahan−Starling equation of state[35] for hard spheres. We have picked the reference state for nanoparticles as in de Luzuriaga et al.:[17] ϕ_f is the maximum packing of disordered, "molten" spheres in vacuum (ϕ_f = 0.494). We have not included terms describing the loss in conformational entropy of chains due to stretching[14,18] and/or compression[17] induced by confinement among nanoparticles. Including these terms as formulated by Mackay et al.[14] simply lowers our estimation of the phase boundary for demixing a very minor amount. They evidently do not play a crucial role in our system. The first and third terms on the right of eq 3 imply exchange between bound and matrix polymer fractions; the matrix polymer fraction gains translational entropy upon mixing from the volume occupied by particles, while the bound polymer fraction contributes a translational entropy of mixing from the particle to which it is adsorbed.

The last term on the right side of eq 3 adds a correction in virial-form to the hard-sphere interactions implied by the third term, which arise from the attractive van der Waals interactions among nanoparticles. This is, in effect, a lowest order correction from a "high temperature expansion"[36] for a long-ranged, weak attractive contribution to the interparticle potential. We employ a pairwise additive estimate for the van der Waals interaction between two spheres[37] to estimate the associated excluded volume parameters b_i:

$$b_i = \frac{-4\pi A_i}{6k_BT}\int_{LB_i}^{\infty} r^2\left[\frac{2R^2}{r^2-4R^2}+\frac{2R^2}{r^2}+\ln\frac{r^2-4R^2}{r^2}\right]dr \quad (4)$$

Note that $b_i < 0$. The reference state (subscript i = f) employs the Hamaker constant $A_f \cong 6.5 \times 10^{-22}$ J, appropriate for silica against vacuum. The lower bound of integration LB_f corresponds to the particle diameter plus a few angstroms of surface roughness. For the mixed state (i = mix) we employ $A_{mix} \cong 1.4 \times 10^{-20}$ J, appropriate for silica against PMA, and put LB_{mix} to be above LB_f by 2δ in the case of particles with a bound polymer layer. This accounts for the steric protection from direct particle−particle contact afforded by a bound layer and screens interparticle attractions at close range.[37] The model applies to the "aggressive thermal annealing" case by setting $k_BT = 5.8 \times 10^{-21}$ J in eq 4. Note that for unfavorable polymer segment−particle surface site interactions $\chi_{2P} \geq 0$, and no polymer adsorbs (δ= 0), so that eq 3 is simplified by putting α = 1. On the other hand, if χ_{2P} is sufficiently negative, that is for sufficiently favorable polymer segment−surface site interactions, polymer adsorption from the melt onto nanoparticles does occur, making $\delta > 0$. Then the model predicts a reduction in the (favorable) translational entropy of mixing. The phase boundary was found by determining the largest value of χ_{2P} at each ϕ_P that satisfied the conditions

$$\Theta < 0 \quad \text{and} \quad \frac{d^2\Theta}{d\phi_P{}^2} > 0 \quad (5)$$

The resulting phase boundaries for two fixed values of δ are shown in Figure 6a. With no bound layer (δ = 0), relevant only for $\chi_{2P} \geq 0$, the model predicts miscibility only for χ_{2P} below a very small positive value. In this region the mixed state is favorable since the gain in translational entropy upon mixing dominates over (relatively small) interparticle attraction and weak unfavorable segment−surface site enthalpy terms. This case is likely not realistic for our system, however, since PMA is reported to adsorb onto silica,[22,24] suggesting that χ_{2P} is actually negative and therefore that $\delta > 0$. The presence of a substantial bound layer, say of thickness δ = 1.7 nm, which is a realistic value for our system, reduces the net translational entropy gain upon mixing significantly and shifts the phase boundary as illustrated in Figure 6a. The estimation of δ = 1.7 nm was drawn from an observed trend in differential scanning calorimetry experiments that was corroborated by literature data. Details can be found in Appendix B of the Supporting Information. We emphasize that the energetics of adsorption, which are favorable to mixing, are taken into consideration properly in Figure 6a by a phase boundary following the curves drawn for $\delta = 0$ if $\chi_{2P} \geq 0$, but with δ a positive, constant value if the polymer/particle interaction parameter is negative. Now, for our system, undergoing "aggressive thermal annealing" (i.e., for observation (i)), we estimate the polymer segment/particle surface interaction parameter as $\chi_{2P} \approx -0.3$, from a sum[38] of hydrogen bonding[39] and dispersive[38,40,41] interaction contributions. Figure 6a indicates that the model predicts miscibility for the range of ϕ_P we studied, consistent with our observations. In particular, the model suggests that interparticle

attractions, which are unfavorable to miscibility, cannot overcome the strong segment−surface energetic interactions represented by the large χ_{2P}, which are favorable to miscibility.

In the previous four paragraphs we introduced a thermodynamic model that examines the effect an adsorbed polymer layer has on PNC miscibility in the context of our experimental results. Next consider observation (ii), of demixing of well-dispersed samples upon exposure to a solvent/displacer. It is appropriate here to neglect a bound layer ($\delta = 0$). This situation requires treatment of a ternary system composed of nanoparticles, solvent, and (unbound) polymer, denoted components P, 1, and 2, respectively, with respective volume fractions ϕ_P°, $\phi_1^\circ(1 - \phi_P^\circ)$, and $(1 - \phi_1^\circ)(1 - \phi_P^\circ)$. ϕ_P° is the volume fraction of nanoparticles in the ternary system, which we note is different than the volume fraction of nanoparticles in the dry PNC, ϕ_P. It can be shown that $\phi_P^\circ = \phi_P(1 - \phi_1^\circ)(1 - \phi_P\phi_1^\circ)^{-1}$, where ϕ_1° is the volume fraction of solvent in the polymer. We adapted terms from the ternary theory by He et al.[18] for a polymer blend with added nanoparticles to this case by setting $N = 1$ for one component in the blend, making it represent the solvent/displacer. The resulting expression for ΔF is

$$\frac{v_0\Delta F}{Vk_BT} = \Theta = \frac{(1-\phi_1^\circ)(1-\phi_P^\circ)}{N}\ln((1-\phi_1^\circ)(1-\phi_P^\circ)) + (1-\phi_P^\circ)\phi_1^\circ\ln((1-\phi_P^\circ)\phi_1^\circ) + \chi_{12}(1-\phi_P^\circ)^2\phi_1^\circ(1-\phi_1^\circ) + \phi_P^\circ\frac{v_0}{v_P}\left[\ln(\phi_P^\circ) + \frac{4(\phi_P^\circ) - 3(\phi_P^\circ)^2}{(1-\phi_P^\circ)^2} - \ln(\phi_f) - \frac{4\phi_f - 3\phi_f^2}{(1-\phi_f)^2}\right] + \frac{1}{2}\frac{v_0}{v_P}\left[\frac{\phi_P^{\circ 2}}{v_P}b_{mix} - \frac{\phi_P^\circ\phi_f}{v_P}b_f\right] + \chi_{1P}\phi_P^\circ(1-\phi_P^\circ)\phi_1^\circ\frac{r_0}{R} + \chi_{2P}\phi_P^\circ(1-\phi_P^\circ)(1-\phi_1^\circ)\frac{r_0}{R} \quad (6)$$

The first three terms on the right of eq 6 are the Flory−Huggins free energy of mixing for the polymer/solvent pair, where the enthalpic contribution due to polymer segment−solvent interactions is characterized by χ_{12}. The fourth and fifth terms are nearly identical to those in eq 3 and represent contributions from the nanoparticle translational entropy and interactions. The sixth and seventh terms on the right side of eq 3 are the enthalpic contributions from solvent/particle surface and polymer segment/particle surface interactions, as formulated by He et al.,[18] using Flory parameters χ_{1P} and χ_{2P}, respectively.

Representing the effect of ethyl acetate as a good solvent/displacer on the mixture's miscibility puts restrictions on parameters in the model. In eq 4, $k_BT = 4.3 \times 10^{-21}$ J is used. In eq 6 we put $\chi_{12} = 0.4$ as a reasonable value for a "good solvent" and use a large negative value of χ_{2P} as in the previous case ($\chi_{2P} \cong -0.45$ was estimated as mentioned previously[38,39]). Finally, $\chi_{1P} < \chi_{2P}$ is anticipated to represent the displacing nature of the solvent. The spinodal boundary for different values of ϕ_1°, was then found by determining the values of χ_{1P} for various ϕ_P° that satisfied the conditions

$$\Theta < 0, \quad \left(\frac{\partial^2\Theta}{\partial\phi_1^{\circ 2}}\right)\left(\frac{\partial^2\Theta}{\partial\phi_P^{\circ 2}}\right) - \left(\frac{\partial^2\Theta}{\partial\phi_1^\circ\partial\phi_P^\circ}\right)^2 > 0, \quad \frac{\partial^2\Theta}{\partial\phi_1^{\circ 2}} > 0, \quad \frac{\partial^2\Theta}{\phi_P^{\circ 2}} > 0 \quad (7)$$

The results (Figure 6b) show that when the amount of added solvent displacer is low (e.g., $\phi_1^\circ \leq 0.3$), miscibility is predicted for all compositions and reasonable values of the solvent/particle surface interaction parameter χ_{1P} ($-1 < \chi_{1P} < -0.45$). However, since ethyl acetate is a good solvent for PMA,[22] ϕ_1° should be relatively high during the "solvent annealing" procedure. While we did not measure ϕ_1° during solvent annealing, $\phi_1^\circ \geq 0.5$ is consistent with an estimate from Flory−Huggins solution theory for a good solvent ($\chi_{12} = 0.4$) at near unit solvent activity ($a_1 \geq 0.9$). For $\phi_1^\circ = 0.5$, miscibility is only predicted when ϕ_P° is either very high or very low. The region of miscibility at high ϕ_P° is roughly $\phi_P > 0.4$, and the lower region of miscibility is transcendentally small, beyond experimental resolution. According to the model, the addition of such large amounts of displacing solvent make the mixed state entropically unstable (i.e., the third term in eq 6 causes the second miscibility condition in eq 7 to be violated). Thus, the experimentally observed demixing after exposure to the displacing solvent (e.g., Figure 1c) is anticipated by the model.

V. CONCLUSIONS AND DISCUSSION

Sample history is a critical factor influencing nanoparticle dispersion in the PMA/SiO_2 system according to SAXS and TEM evidence. Samples cast from a mutually good solvent, which is also a displacer, and then dried show particle-rich and particle-lean regions (or "phases") in coexistence. However, a random dispersion was observed for these same samples after they had been thermally annealed at a relatively high temperature for an extended time period, indicative of miscibility of the melt and nanoparticles under these conditions. Analysis with a mean-field thermodynamic model that accounts for an adsorbed polymer layer around each nanoparticle showed that the observed miscibility for thermally annealed samples is satisfactorily explained by strong, energetically favorable polymer segment/nanoparticle surface interactions. Implicit in this explanation is the assumption that the morphologies observed in quench-cooled or rapidly dried samples are those at the annealing conditions, but kinetically arrested at room temperature. Essentially similar results have been observed by Harton et al.[26] for PNCs made from poly(2-vinylpyridine) and silica.

For these thermally annealed samples, subsequent exposure to a good solvent able to displace adsorbed PMA chains from the SiO_2 surface evidently caused demixing. This is consistent with the thermodynamic analysis of a ternary system, which predicts immiscibility when significant amounts of the displacing solvent is present via entropic destabilization. The agreement between experiments and theory for this case is reminiscent of observations by Kim et al. on PNCs made from spherical silica particles of $d = 44$ nm and poly(ethylene glycol) (PEG, MW = 400).[20] In that work, the dry PNC was miscible, while adding the good solvent ethanol displaced the polymer and resulted in nanoparticle aggregation. The apparent reversibility of our nanoparticle dispersion from a phase-separated morphology to a randomly dispersed one and back suggests the possibility of optimizing sample history to tailor nanoparticle dispersion for applications.

■ ASSOCIATED CONTENT

Supporting Information. A brief review of the model used in the analysis of SAXS data, a discussion of the physical meaning of the model parameters, and the details of the regression fitting process (Appendix A); an estimation of particle volume faction and bound layer thickness from thermal gravimetric analysis and differential scanning calorimetry (Appendix B).

This material is available free of charge via the Internet at http://pubs.acs.org.

AUTHOR INFORMATION

Corresponding Author
*E-mail cjd2@columbia.edu; Ph (212) 854-8161.

ACKNOWLEDGMENT

The authors thank X27C beamline scientists Lixia Rong and Jie Zhu for training and instrument setup as well as Professor Sanat Kumar for helpful discussions. Also, D.W.J. gratefully thanks the National Science Foundation for funding through the IGERT Program for the Study of Multiscale Phenomena in Soft Materials. Use of the National Synchrotron Light Source, Brookhaven National Laboratory, was supported by the U.S. Department of Energy, Office of Science, Office of Basic Energy Sciences, under Contract DE-AC02-98CH10886. This work has used the shared experimental facilities that are supported primarily by the MRSEC Program of the National Science Foundation under Award DMR-0123574 and by the New York State Office of Science Technology and Academic Research (NYSTAR). Partial funding for this research was provided by the National Science Foundation Division of Materials Research (J.F.M., NSF DMR-0804647).

REFERENCES

(1) Hussain, F.; Hojjati, M.; Okamoto, M.; Gorga, R. E. *J. Compos. Mater.* **2006**, *40*, 1511–1575.
(2) Crosby, A. J.; Lee, J.-Y. *Polym. Rev.* **2007**, *47*, 217–229.
(3) Okada, A.; Usuki, A. *Macromol. Mater. Eng.* **2006**, *291*, 1449–1476.
(4) Ray, S.; Easteal, A. J. *Mater. Manuf. Processes* **2007**, *22*, 741–749.
(5) Takahashi, S.; Paul, D. R. *Polymer* **2006**, *47*, 7519–7534.
(6) Takahashi, S.; Paul, D. R. *Polymer* **2006**, *47*, 7535–7547.
(7) Akcora, P.; Kumar, S. K.; Moll, J.; Lewis, S.; Schadler, L. S.; Li, Y.; Benicewicz, B. C.; Sandy, A.; Narayanan, S.; Ilavsky, J.; Thiyagarajan, P.; Colby, R. H.; Douglas, J. F. *Macromolecules* **2010**, *43*, 1003–1010.
(8) Beek, W. J. E.; Janssen, R. A. J. Hybrid Polymer-Inorganic Photovoltaic Cells. In *Hybrid Nanocomposites for Nanotechnology*; Merhari, L., Ed.; Springer Science + Business Media: New York, 2009; pp 321−385.
(9) Schaefer, D. W.; Justice, R. S. *Macromolecules* **2007**, *40*, 8501–8517.
(10) Rong, M. Z.; Zhang, M. Q.; Ruan, W. H. *Mater. Sci. Technol.* **2006**, *22*, 787–796.
(11) Hooper, J. B.; Schweizer, K. S. *Macromolecules* **2006**, *39*, 5133–5142.
(12) Akora, P.; Liu, H.; Kumar, S. K.; Moll, J.; Li, Y.; Benicewicz, B. C.; Schadler, L. S.; Acehan, D.; Panagiotopoulos, A. Z.; Pryamitsyn, V.; Ganesan, V.; Ilavsky, J.; Thiyagarajan, P.; Colby, R. H.; Douglas, J. F. *Nature Mater.* **2009**, *8*, 354–359.
(13) Meier, D. J. *J. Phys. Chem.* **1967**, *71*, 1861–1868.
(14) Mackay, M. E.; Tuteja, A.; Duxbury, P. M.; Hawker, C. J.; Van Horn, B.; Guan, Z.; Chen, G.; Krishnan, R. S. *Science* **2006**, *311*, 1740–1743.
(15) Harton, S. E.; Kumar, S. K. *J. Polym. Sci., Part B: Polym. Phys.* **2008**, *46*, 351–358.
(16) Ginzburg, V. V. *Macromolecules* **2005**, *38*, 2362–2367.
(17) de Luzuriaga, A. R.; Etxeberria, A.; Rodriguez, J.; Pomposo, J. A. *Polym. Adv. Technol.* **2008**, *19*, 756–761.
(18) He, G.; Ginzburg, V. V.; Balazs, A. C. *J. Polym. Sci., Part B: Polym. Phys.* **2006**, *44*, 2389–2403.
(19) Hall, L. M.; Anderson, B. J.; Zukoski, C. F.; Schweizer, K. S. *Macromolecules* **2009**, *42*, 8435–8432.
(20) Kim, S. Y.; Hall, L. M.; Schweizer, K. S.; Zukoski, C. F. *Macromolecules* **2010**, *43*, 10123–10131.
(21) de Luzuriaga, A. R.; Grande, H. J.; Pomposo, J. A. *J. Chem. Phys.* **2009**, *130*, 084905.
(22) Kamiyama, F.; Inagaki, H. *Bull. Inst. Chem. Res, Kyoto Univ.* **1974**, *52*, 393–402.
(23) Kulkeratiyut, S.; Kulkeratiyut, S.; Blum, F. D. *J. Polym. Sci., Part B: Polym. Phys.* **2006**, *44*, 2071–2078.
(24) Metin, B.; Blum, F. D. *J. Chem. Phys.* **2006**, *125*, 054707.
(25) Xia, J.; Matyjaszewski, K. *Macromolecules* **1997**, *30*, 7697–7700.
(26) Harton, S. E.; Kumar, S. K.; Yang, H.; Koga, T.; Hicks, K.; Lee, H. K.; Mijovic, J.; Liu, M.; Vallery, R. S.; Gidley, D. W. *Macromolecules* **2010**, *43*, 3415–3421.
(27) Bansal, A.; Yang, H.; Li, C.; Cho, K.; Benicewicz, B. C.; Kumar, S. K.; Schadler, L. S. *Nature Mater.* **2005**, *4*, 693–698.
(28) Roe, R.-J. *Methods of X-Ray and Neutron Scattering in Polymer Science*; Oxford University Press: New York, 2000.
(29) Beaucage, G.; Ulibarri, T. A.; Black, E. P.; Schaefer, D. W. Multiple size scale structures in silica-siloxane composites studied by small-angle scattering. In *Hybrid Organic-Inorganic Composites*; Mark, J. E., Lee, C. Y.-C., Bianconi, P. A., Eds.; American Chemical Society: Washington, DC, 1995; Vol. 585, pp 97−111.
(30) Chen, C.; Justice, R. S.; Schaefer, D. W.; Baur, J. W. *Polymer* **2008**, *49*, 3805–3815.
(31) Beaucage, G.; Kammler, H. K.; Pratsinis, S. E. *J. Appl. Crystallogr.* **2004**, *37*, 523–535.
(32) Demyanchuk, I.; Wieczorek, S. A.; Hołyst, R. *J. Chem. Phys.* **2004**, *121*, 1141–1147.
(33) Yaklin, M. A.; Duxbury, P. M.; Mackay, M. E. *Soft Matter* **2008**, *4*, 2441–2447.
(34) Rodriguez, A. E. *Proc. R. Soc. London, Ser. A* **1949**, *196*, 73–92.
(35) Carnahan, N. F.; Starling, K. E. *J. Chem. Phys.* **1969**, *51*, 635–636.
(36) Hansen, J. P.; McDonald, I. R. *Theory of Simple Liquids*; Academic Press, Inc.: New York, 1976.
(37) Russel, W. B.; Saville, D. A.; Schowalter, W. R. *Colloidal Dispersions*; Cambridge University Press: Cambridge, 1989.
(38) Coleman, M. M.; Serman, C. J.; Bhagwagar, D. E.; Painter, P. C. *Polymer* **1990**, *31*, 1187–1203.
(39) Zhang, S.; Painter, P. C.; Runt, J. *Macromolecules* **2004**, *37*, 2636–2642.
(40) Schoenmakers, P. J.; Billiet, H. A. H.; de Galan, L. *Chromatographia* **1982**, *15*, 387–398.
(41) Brandrup, J.; Immergut, E. H.; Grulke, E. A.; Abe, A.; Bloch, D. R. *Polymer Handbook*, 4th ed.; John Wiley & Sons: Hoboken, NJ, 2005.